

Numerical Optimization for Source-Drain Channel Resistance of AlGa_N/Ga_N HEMTs

Rajab Yahyazadeh^{1*}, Zahra Hashempour¹

¹Department of Physics, Khoy Branch, Islamic Azad University, Khoy, Iran P.O.Box: 175-58135

*Corresponding Author

DOI: <https://doi.org/10.30880/jst.2019.11.01.001>

Received 1 January 2019; Accepted 1 June 2019; Available online 10 June 2019

Abstract: A numerical model for the source-drain channel resistance based high electron mobility transistors has been developed that is capable to predict accurately the effects of polarization Coulomb Field Scattering (PCF), multi sub-band on source-drain channel resistance. Salient features of the model are incorporated of fully and partially occupied sub-bands in the interface quantum well, combined with a self-consistent solution of the Schrödinger and Poisson equations. In addition, to develop the model, accurate two-dimensional electron gas mobility and modified wave function in barrier AlGa_N have been used. According to the numerical calculations, the effect of multi sub-band and PCF scattering on the increase of source-drain channel resistance is 35% and 65%, respectively, with the effect of PCF being almost twice as high as multi sub-band. The calculated model results are in very good agreement with existing experimental data for high electron mobility transistors device.

Keywords: PCF scattering, multi sub-band, channel resistance

1. Introduction

GaN high electron mobility transistors (HEMTs) are used in high frequency, high power, and robust low-noise applications [1–3]. Linearity is one of the most crucial figures of merit for the application of power amplifiers. For improving the device linearity, advanced device structures or epitaxial structure engineering, such as field plate, nonlinear polarization dielectric, double-channel, and optimized barrier or cap layer thickness, have been explored [4–7]. Polarization Coulomb Field (PCF) scattering, which stems from the non-uniform distribution of the polarization charges at the AlGa_N/Ga_N interface, is a particular scattering mechanism in AlGa_N/Ga_N HFETs. It has been reported that PCF scattering can affect electron mobility and parasitic source access resistance (R_S) [8–9]. Besides, III–V nitride-based HEMTs simulations show that the Polarization Coulomb Field Scattering plays a very important role in limiting the device performance, especially saturation region [10,11]. However, the high power dissipation of AlGa_N/Ga_N HEMTs operating at large biases may result in high junction temperature and enhance the phonon scattering causing a drop in carrier mobility. This effect has been reported to be of great influence on the static current characteristics and is commonly referred to as self-heating. The evidence of such an effect is a negative slope of drain current I_{DS} versus drain voltage V_{DS} [12]. More recently, the source-drain channel resistance of III nitride-based HEMT has been modeled by several groups analytically, numerically or analytical-numerically [12–14]. It is important to investigate systematically the dependence of AlGa_N–Ga_N HEMT performance on the Polarization Coulomb Field Scattering and multi sub-band with including different physical parameters. In this paper, we report the results on the effects of Polarization Coulomb Field Scattering on the parasitic and channel resistance with including multi sub-band. The channel resistance of these transistors was previously calculated without including PCF scattering [16]. In the present work, a new numerical model for total resistance is presented. That is capable of determining effects of PCF scattering and multi sub-band on the parasitic and channel resistance. This is achieved by (i) using a self-consistent solution of the Schrödinger and Poisson equations in order to obtain both two-dimensional electron gas density, wave

function, Fermi level (E_{Fi}) specified relative to the bottom of a triangular well, (ii) take into account the modified wave function in the AlGa_N barrier, (iii) take into account the occupancy of the various sub-bands, the intrasubband, and intersubband coupling coefficients H_{mn} . The fringing-field effect can be ignored in the present numerical model.

2. Material and Method

In order to obtain accurate values for the Fermi energy, the energies of quantized levels within the 2DEG, the occupancy of the various sub-bands, the intrasubband and intersubband coupling coefficients, potential profiles, wave function and the sheet carrier concentration for the 2DEG in AlGa_N/Ga_N heterostructures; both the Schrödinger and Poisson equations must be solved self-consistently. This has been achieved by solving Schrödinger's equation and simultaneously taking into account the electrostatic potential obtained from Poisson's equation, as well as the image and exchange-correlation potentials using Numerov's numerical method. In the self-consistent calculation, the nonlinear formalism of the polarization-induced field as a function of Al mole fraction in AlGa_N/Ga_N heterostructures have been assumed, as well as taking into account all fully and partially occupied sub-bands within the interface 2DEG potential well [13,15]. Using such an approach, it is possible to calculate the 2D-electron mobility taking into account the combined contributions from each of the individual electron scattering mechanisms [16]. The field-effect transistor (FET) model used in calculations is shown schematically in Fig. 1. Knowing the electron energy in any sub-band (E_i), the 2DEG density (n_{2D}), and the Fermi energy can be calculated [12, 16, 18, and 19]. The Quantum correction for the effective width of the 2DEG ($\Delta d_{2DEG} = 1/n_{2D} \int z n_{2D}(z) dz$) at a different electron temperature (T_e) is given by [20]:

$$\Delta d_{2DEG} = 5.6 \times 10^{-9} T_e + 4.7 \times 10^{-8} \quad (1)$$

Knowing the behavior of the 2DEG density as a function of the gate voltage, one can obtain the 2D electron mobility as a function of the gate voltage along the channel [21]. On the other hand, from the charge transport model, the channel potential is well known for AlGa_N/Ga_N heterostructure FETs. Hence the electron temperature can be derived from the energy balance model as [22]

$$T_e = T_0 + \left(\frac{2e}{3k_B}\right) \tau_{total} \mu_{2DEG} F^2 \quad (2)$$

where τ_{total} is the total relaxation time, K_B is the Boltzmann constant, T_0 is the lattice temperature, μ_{2DEG} is the electron mobility and F is the electric field along the 2DEG channel.

The additional polarization charge ($\Delta\sigma$) in the gate region can be calculated as the following relation [23]:

$$\Delta\sigma = \frac{e_{33}^2}{C_{33}} \Delta E_z^{AlGaN} \quad (3)$$

Here, e_{33} , C_{33} and n_{2D} are the piezoelectric coefficients, the elastic stiffness tensor and barrier thickness of AlGa_N, respectively, $\Delta E_z^{AlGaN} = (V_{GS} - V_{CH}) / d_{AlGaN}$ is the vertical direction electric field across the AlGa_N barrier layer. ΔE_z^{AlGaN} and $\Delta\sigma$ under the various gate-source voltage V_{GS} and channel potential V_{CH} are calculated using Eq. (3). The energy-dependent momentum relaxation rate $1/\tau_{PCF}$ for PCF scattering can be written as [21,24]:

$$\frac{1}{\tau_{PCF}} = \frac{Am^*}{2\pi\hbar^2} \int_0^\pi \left[\frac{M_{K-K'}}{S(q, T_e)} \right] (1 - \cos\theta) d\theta \quad (4)$$

where A is the 2-D normalization constant that converts the scattering rate per area and θ is the scattering angle between initial state k and final state k' . $S(q, T_e)$ is the screening function to reflect the screening effect and $M_{K-K'}$ is the matrix element (depend on the wave function) for the transition from initial state k to the final state k' [24]. The wave function, although being very practical for most of the relevant mobility-related calculation, has the drawback of being zero in the barrier region. This is equivalent to consider the barrier as infinitely high. However, alloy scattering is a mobility-limiting mechanism intrinsically related to the penetration wave function in the barrier region. This can be overcome by using a modified Fang-Howard wave function [25]. Besides PCF scattering, the other main scattering mechanisms are polar-optical-phonon (POP) scattering, piezoelectric (PE) scattering, alloy scattering (Alloy), dislocation scattering (DIS), acoustic-phonon (AP), and interface roughness (IFR) scattering [26-29,16]. The

momentum relaxation time τ_{IFR} , τ_{DIS} , τ_{POP} , τ_{Alloy} , τ_{AP} and τ_{PE} can be calculated using the pre-existing calculation formula [11,24]. By Matthiessens rule, R_C and R_D can be written as:

$$R_S = \frac{m^*(L_{GS})}{n_{2D0}e^2W_G} \left(\frac{1}{\tau_{PCF}} + \frac{1}{\tau_{POP}^F} + \frac{1}{\tau_{AP}^F} + \frac{1}{\tau_{IFR}^F} + \frac{1}{\tau_{DIS}^F} + \frac{1}{\tau_{Alloy}^F} \right) \quad (5)$$

$$R_S = \frac{m^*(L_{GD})}{n_{2D0}e^2W_G} \left(\frac{1}{\tau_{PCF}} + \frac{1}{\tau_{POP}^F} + \frac{1}{\tau_{AP}^F} + \frac{1}{\tau_{IFR}^F} + \frac{1}{\tau_{DIS}^F} + \frac{1}{\tau_{Alloy}^F} \right) \quad (6)$$

If $L_{GS} = L_{GD}$ than $R_S = R_D$

$$R_{CH} = R_G = \frac{m^*(L_G)}{n_{2D}e^2W_G} \left(\frac{1}{\tau_{PCF}} + \frac{1}{\tau_{POP}^G} + \frac{1}{\tau_{AP}^G} + \frac{1}{\tau_{IFR}^G} + \frac{1}{\tau_{DIS}^G} + \frac{1}{\tau_{Alloy}^G} \right) \quad (7)$$

$$R_{total} = R_G + R_F + 2R_C, \quad R_F = R_S + R_D, \quad R_{CH} = R_G \quad (8)$$

The contact resistance R_C is constant and R_S is of different value during the measurement. As a result, R_S is determined by the scattering mechanisms for the electrons in the gate-source channel [27]. In order to obtain accurate values for mobility, the nonlinear formalism of the polarization-induced field as a function of Al mole fraction in Al_mGa_{1-m}N/GaN HEMTs have been assumed, as well as taking into account intersubband coupling coefficients $H_{mn} = \iint dz_1 dz_2 \psi_{mn}(z_1) \psi_{mn}(z_2) \times \exp(q|z_1 - z_2|)$ and all fully and partially-occupied sub-bands within the interface 2DEG potential well. From the definition of the drift mobility we obtain [26-28]:

$$\mu_{2DEG}(T_e, E) = \frac{e}{m^*} \langle \tau_{total}(T_e, E) \rangle \quad (9)$$

where τ_{total} are the total relaxation times associated with PCF scattering and the other main scattering mechanisms so that these relaxation times have been calculated using the methods described in Refs [26-29, 16]. Also, the different scattering rates can be separated into two types: (i) elastic scattering due to acoustic and piezoelectric phonons, ionized impurities and interface roughness, etc., and (ii) inelastic scattering due to polar optical phonons. In order to take into consideration all scattering mechanisms in the mobility calculation, it is necessary to include all such mechanisms in the linearized Boltzmann equation and to solve it numerically using an iterative technique [9]. It should be noted that in the linearized Boltzmann equation, $\Phi(E, T)$ is the perturbation function so that to obtain the $\Phi(E, T)$ needs to take into account the contribution of all occupied sub-bands by means of following relation [16]:

$$\frac{1}{\Phi(E, T_e)} = \sum_m \sum_n \frac{n_m}{n_{2DEG}} \frac{1}{\Phi_{mn}} \quad (10)$$

Eq. (10) indicated that all occupied states contribute to the total mobility of the two-dimensional electron gases. This equation also shows that the contribution of each sub-band depends on its occupation number (that is relative concentration n_m / n_{2DEG}) such that the most significant contribution comes from the first sub-band, which has the highest occupation number. Using such an approach, it is possible to calculate the 2D-electron mobility taking into account the combined contributions from each of the individual electron scattering mechanisms. Table 1 is the material parameters used in numerical calculation method for 2DEG (Two Dimensional Electron Gas), 2DEM (Two Dimensional Electron Mobility) and Table 2 is the Specific polarization charge values for calculation of the PCF scattering potential ($V(x, y, z)$), $\Delta\sigma$, $M_{K-K'}$ and τ_{PCF} ($\tau_{PCF} = \int [\tau_{PCF}(E)E(\partial f_0(E) / \partial E) dE] / \int [E(\partial f_0(E) / \partial E) dE]$)

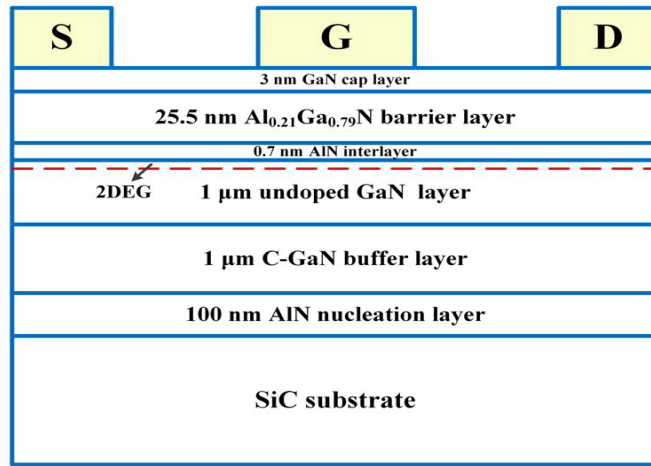


Fig. 1 - Cross-sectional view of the AlGaN/GaN HFETs

3. Results and Discussion

To assess the validity of the numerical model, a comparative study has been undertaken to theoretically compare the obtained results with experimental results. The material parameters used in the 2DEG, 2DEM calculations and specific polarization charge values for AlGaN/GaN HEMTs are presented in Table 1 and 2. Moreover, all other material parameters and device details have been taken from Refs. [10, 17, 20, 30 and 31] for $Al_{0.21}Ga_{0.79}N/GaN$ HEMTs. Fig. 2 shows that as L_G increases, the 2-DEG density (n_{2D}) decreases and the threshold voltage shifts towards increasingly negative values. The large values n_{2D} are attributed to the presence of polarization induced charges in AlGaN/GaN HEMTs, which have been incorporated accurately in the proposed model. The slope of the $n_{2D} - V_{GS}$ curves corresponds to the capacitance of the structure, which is related directly to the separation between the gate and 2DEG, i.e., the thickness of the AlGaN layer. As L_G decreases, the slope of the $n_{2D} - V_{GS}$ curves slightly increases beyond the threshold. This is due to the fact that the gate capacitance decreases as L_G decreases. For $L_G = 4\mu m$, the slope is obtained as $1.9551012cm^{-2}V^{-1}$, whereas for $L_G = 16\mu m$, the slope decreases to $1.81012cm^{-2}V^{-1}$. Thus, a lower value L_G is desirable to achieve a high value of the 2-DEG density and lower values of the gate capacitance. The wave functions under different n_{2D} , as shown in Fig. 3. It is apparent that the wave function is closely relevant to n_{2D} . The greater n_{2D} helps the electron wave to well-function in the quantum, and the modified Fang-Howard (inset of Fig. 3) is closer to the AlGaN/GaN interface. Hence, the wave function depends on n_{2D} . In Fig. 3 and 4, Calculated specific R_S and R_D as a function of forward gate-source voltage for PCF, POP, AP, IFR, ALLOY and DIS scatterings as well as the total R_S (TOTAL) and the measured R_S values at room temperature in comparison with experimental data. As shown in Fig. 5, only the resistance of PCF with the gate voltage is changed, which is related to the polarization charge $\Delta\sigma$ in the gate region. The rest of the resistors are fixed at the gate voltage, except for the resistance POP, which is extremely small in relation to the voltage and thus is not effective in the variation process of R_S (or R_D at this temperature. However, this will be effective at high temperatures, although investigation in this study was performed only at the 300K temperature. Fig. 5 shows how this issue is corrected. The calculated R_{total} for devices is shown in Fig. 5. As shown in the figure, there is a distinct difference between the experimental data and the calculated R_{total} excluding the PCF scattering and the MSB effect. This means that the PCF scattering and the MSB effect are not ignorable in AlGaN/GaN HEMTs. The effect of the MSB and PCF scattering on increasing the source-drain channel resistance is almost 35% and 65%, respectively. However, the increase in V_{GS} and thus the decrease in the electric potential in the channel under the gate induces the decrease/increase in the negative/positive $\Delta\sigma$, according to Eq. (3). Accordingly, the PCF scattering becomes weaker with the increase in V_{GS} , inducing a decrease in R_{total} .

Table 1- Material parameters used in 2DEG and mobility calculations for the $Al_{0.21}Ga_{0.79}N / GaN$ HEMTs (Refs. 10, 14, 19–21)

Parameters	Unit	Value
Electron effective mass m_{GaN}^*	m_0	0.228
Mass density	kg / m^3	6.13103
Static dielectric constant $\epsilon_S(GaN)$	ϵ_0	10.4
Optical dielectric constant ϵ_∞	ϵ_0	5.35
LO-phonon energy	meV	90.5
Acoustic-phonon velocity	m / s	6.6×10^3
Piezoelectric constant h_{14}	V / m	4.28×10^9
Deformation potential	eV	8.5
Elastic constant C_L	N / m^2	2.66×10^{11}
Elastic constant C_T	N / m^2	0.66×10^{11}
Band gap $E_g^{GaN}(0)$	eV	3.42
Band gap $E_g^{AlN}(0)$	eV	6.13
Drain-gate & gate-source distance (LGD & LGS)	μm	8
gate with	μm	100
Gate length	μm	4
AlGaIn unintentional doping density	cm^{-3}	1×10^{18}
AlGaIn Si doping density	cm^{-3}	2×10^{18}
Electron effective mass $m_{Al_mGa_{1-m}N}^*$	m_0	0.252m+0.228
Static dielectric constant $\epsilon_S(Al_mGa_{1-m}N)$	ϵ_0	-0.3m+10.4
Schottky barrier height $\Phi_B(m)$	eV	1.3m+0.84
Interface roughness parameter L	nm	1.5
Dislocation charge density N_{diss}	cm^{-2}	1×10^{10}
Lattice constant c	Å	5.185
Average displacement of the interface	nm	1
Auto-correction length of Δ	nm	7.5

Table 2- Specific polarization charge values for the PCF scattering potential (Refs. 10, 26)

$V_{GS}(V)$	$\rho_0(10^{-2} C / m^2)$	$\rho_1(10^{-2} C / m^2)$	$\rho_2(10^{-2} C / m^2)$	$\rho_3(10^{-2} C / m^2)$	$\rho_4(10^{-2} C / m^2)$
0.6			1.451	1.463	1.453
0.7			1.450	1.465	1.453
0.8			1.450	1.466	1.452
0.9	1.455	0	1.449	1.467	1.452
1.0			1.448	1.469	1.452
1.1			1.447	1.470	1.451

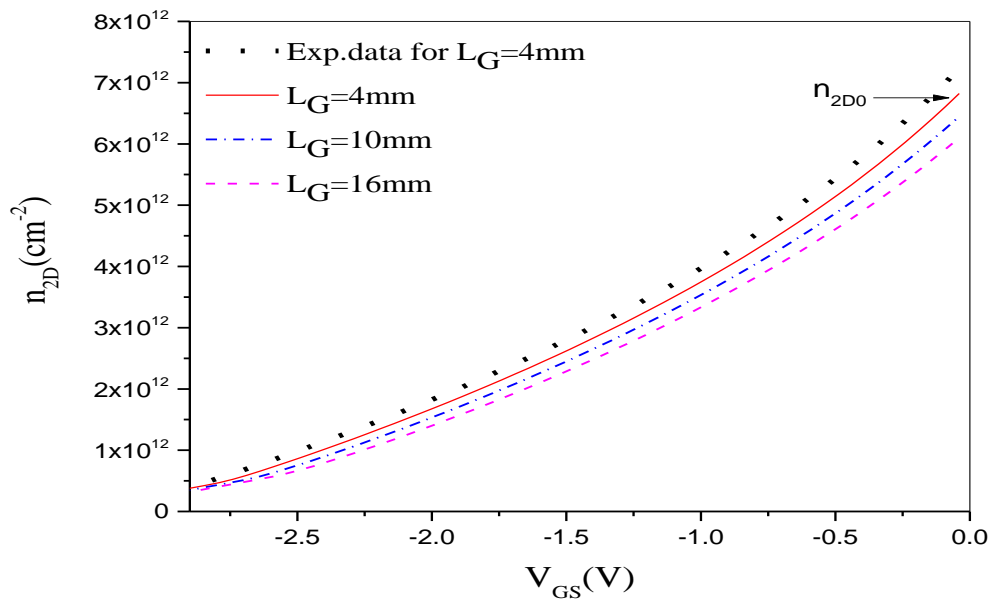


Fig. 2 - The 2DEG density (n_{2D}) verse V_{GS} for $Al_{0.21}Ga_{0.79}N / GaN$ HEMTs with different gate lengths in comparison with experimental data [31].

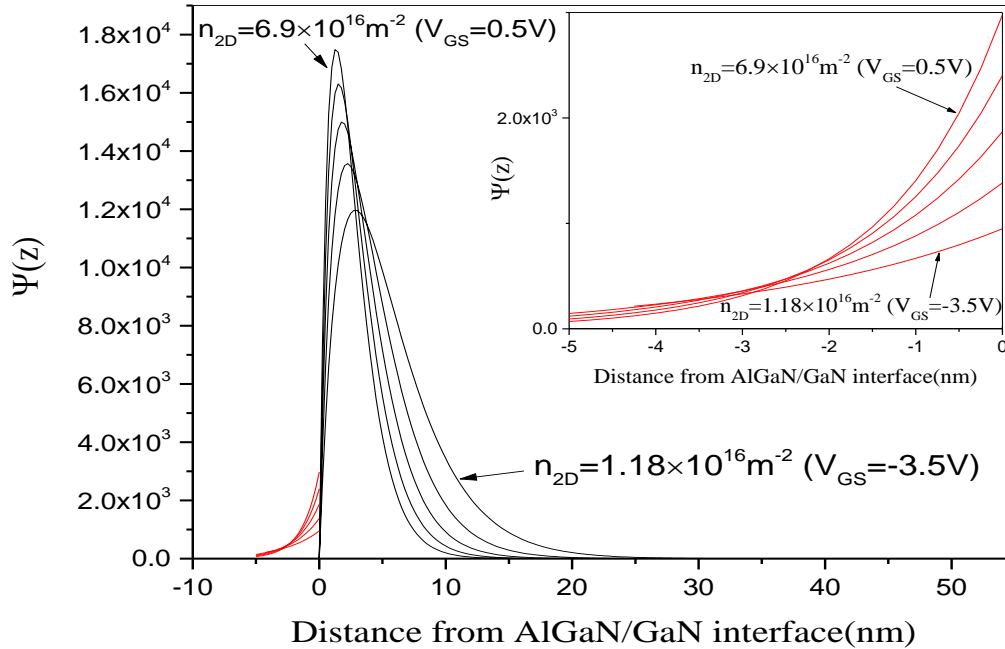


Fig. 3 - The electron wave function $\psi(z)$ as a function of the distance from $Al_{0.21}Ga_{0.79}N / GaN$ interface under different n_{2D} (here n_{2D} corresponds to the electron density under the gate region as a function of gate bias).

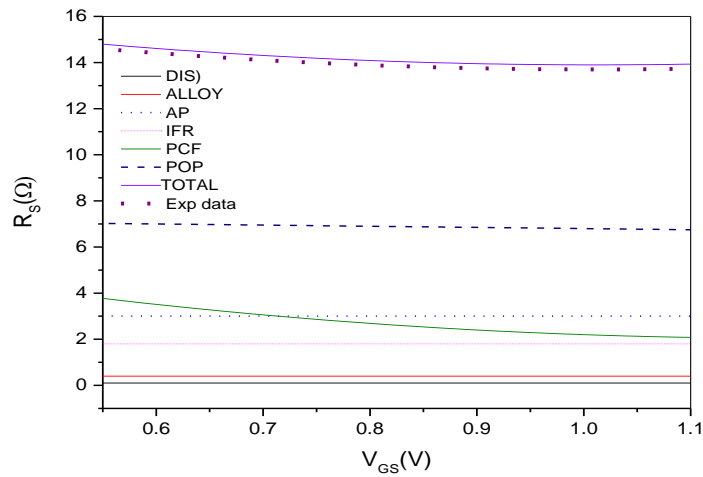


Fig. 4 - Calculated specific R_S as a function of the forward gate-source voltage for PCF, POP, AP, IFR, ALLOY and DIS scatterings as well as the total R_S (TOTAL) and the measured R_S values (the MEASURED) at room temperature in comparison with experimental data [10].

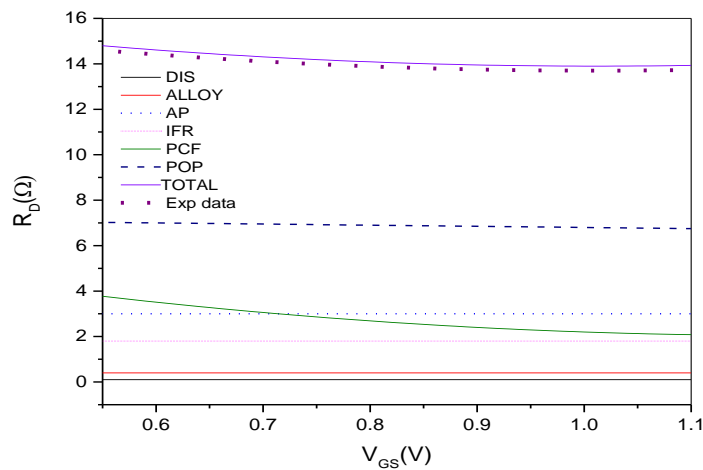


Fig. 5 - Calculated specific R_D as a function of the forward gate-source voltage for PCF, POP, AP, IFR, ALLOY and DIS scatterings as well as the total R_D (TOTAL) and the measured R_S values (the MEASURED) at room temperature in comparison with experimental data [10].

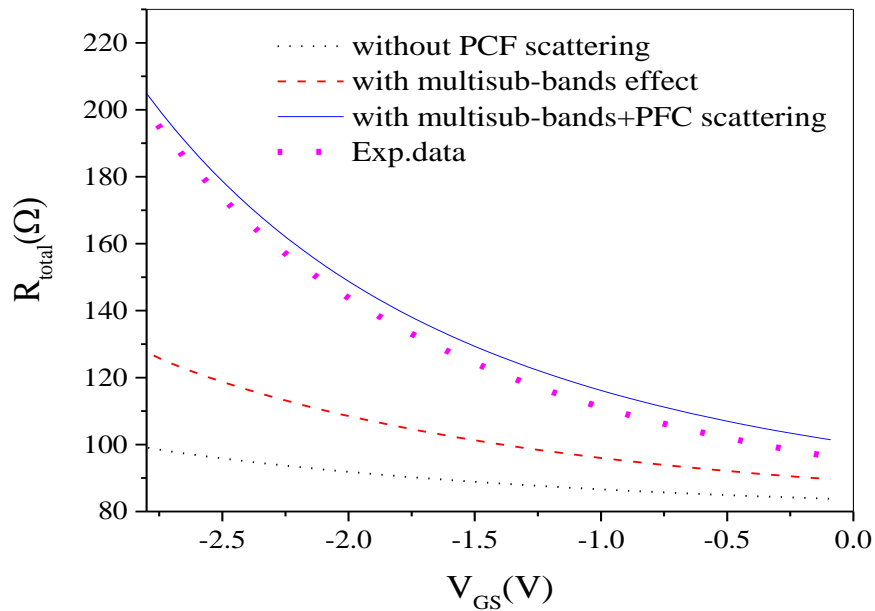


Fig. 5 - Source-drains channel resistance without PCF scattering effect (dot line), with a multi sub-band effect (dashed line) and with all effect (solid line) in comparison with experimental data for $Al_{0.21}Ga_{0.79}N/GaN$ HEMTs [31].

4. Conclusions

In this paper, an accurate numerical model for source-drain channel resistance has been developed for the AlGa_N/Ga_N-based HEMTs. This model is able to accurately predict the dependence of source-drain channel resistance on the PCF scattering, multi sub-band. Calculated specific R_S and R_D as a function of forward gate-source voltage and PCF scattering and multi sub-band effect are not ignorable in source-drain channel resistance AlGa_N/Ga_N HEMTs. According to the numerical calculations, the effect of multi sub-band and PCF scattering on the increase of source-drain channel resistance is 35% and 65%, respectively, with the effect of PCF being almost twice as high as multi sub-band. If most electrons are in the first sub-band, the effect of the multi sub-band will be 5% and PCF % 95, and the PCF scattering will have the greatest effect on total resistance.

Acknowledgment

We are a faculty member of Islamic Azad University, Khoy Branch, and all resources are provided to our work through the University. The authors would like to thank Khoy Branch.

References

- [1] A. Jarndal, et al., (2019). Reliable noise modeling of GaN HEMTs for designing low - noise amplifiers. Int J Numer Model. 2585,1-13.
- [2] Ma, J. & Matioli, E. Slanted, (2017). Slanted tri-gates for high-voltage GaN power devices, IEEE Electron Device Lett. 38, 1305–1308.
- [3] G Tang, et al, (2017). Digital integrated circuits on an E-mode GaN power HEMT platform, IEEE Electron Device Lett. 38, 1282–1285.
- [4] M Blaho, et al, (2017). Annealing, temperature, and bias-induced threshold voltage instabilities in integrated E/D-mode InAlN/GaN MOS HEMTs, Appl. Phys. Lett. 111, 033506.

- [5] K Zhang, et al, (2017). High-Linearity AlGaIn/GaN FinFETs for Microwave Power Applications, IEEE Electron Device Lett. 38, 615–618.
- [6] H Chiu, et al, (2017). RF Performance of in Situ SiN_x Gate Dielectric AlGaIn/GaN MISHEMT on 6-in Silicon-On-Insulator Substrate, IEEE Trans. Electron Devices. 64, 4065–4070.
- [7] S Sun, et al, (2016). AlGaIn/GaN metal-insulator-semiconductor high electron mobility transistors with reduced leakage current and enhanced breakdown voltage using aluminum ion implantation, Appl. Phys. Lett. 108, 013507.
- [8] D. F Brown, et al, (2017). Self-Aligned AlGaIn/GaN FinFETs, IEEE Electron Device Lett. 38, 1445–1448.
- [9] L. Yang, et al, (2017). Enhanced gm and fT with High Johnson's Figure-of-Merit in Tin Barrier AlGaIn/GaN HEMTs by TiN-Based Source Contact Ledge, IEEE Electron Device Lett. 38, 1563–1566.
- [10] P.Cui, et al, (2017). Influence of different gate biases and gate lengths on parasitic source access resistance in AlGaIn/GaN heterostructure FETs, IEEE Trans. Electron Devices. 64, 1038–1044.
- [11] P. Cui, et al, (2017). Effect of polarization Coulomb field scattering on device linearity in AlGaIn/GaN heterostructure field-effect transistors, J. Appl. Phys. 122, 124508.
- [12] A. Douara, et al, (2018). Optimization of two - dimensional electron gas characteristics of AlGaIn/GaN high electron mobility transistors, Int J Numer Model. 2518, 1-9.
- [13] R Yahyazadeh., A Asgari A. M Kalafi, (2006). Effect of depletion layer on negative differential conductivity in AlGaIn/GaN high electron mobility transistor, Physica E, 33, 77-82.
- [14] A. Asgari, S. Babanejad, L. Faraone. (2011). Electron mobility, Hall scattering factor and sheet conductivity in AlGaIn/AlN/GaN heterostructures, J. Appl. Phys, 111, 113713.
- [15] V. Fiorentini, F. Brenardini, O. Ambacher, (2002). Evidence for nonlinear macroscopic polarization in III–V nitride alloy heterostructures, J. Appl. Phys. 80, 1204.
- [16] R. yahyazadeh, (2018). Analytical-numerical model for sheet resistance of high electron mobility transistors, Journal of Non - Oxide Glasses, 10, 2, 57 – 63.
- [17] S Kabra, H Kaur, S Haldar, M Gupta, R.S. Gupta, (2008). An analytical drain current model for graded channel cylindrical/surrounding gate MOSFET, Solid-State Electron, 52, 25.
- [18] A. S. Kumar, N. S. Garigapati, D. Sahaa, (2019). Low field mobility in electrostatically evolved AlGaIn/GaN one-dimensional channel from a two-dimensional electron gas system, J. Appl. Phys. 115, 032105.
- [19] P. Roblin, H. Rahdin, (2002) High-speed Heterostructure Devices from Device Concepts to Circuit Modeling, Cambridge University Press, Cambridge, 277.
- [20] M.A. Huque, S.A.E. liza, T.Rahman, S.K.Islam, (2009). Temperature dependent analytical model for current-voltage characteristics of AlGaIn/GaN power HEMT, Solid State Electronics, 53, 3, 341-348.
- [21] N.S.Swamy, A.K.Datta, (2018). Analytical Models for the 2DEG Density, AlGaIn Layer Carrier Density, and Drain Current for AlGaIn/GaN HEMTs, IEEE Transactions on Electron Devices. 65, 936-944.
- [22] Z. Hashempour, et al, (2009). Numerical performance evaluation of AlGaIn/GaN high electron mobility transistors including gate length effects, Physica E, 41, 1517–1521.
- [23] M.Yang, et al, (2018).Determination of the polarization and strain distribution in AlGaIn/GaN heterostructure field-effect transistors, J. Phys. Chem. Solids, 123, 223–227.
- [24] M. N. Gurusinge, S. K. Davidsson, and T. G. Andersson, (2005). Two-dimensional electron mobility limitation mechanisms in Al_x Ga_{1-x} N/GaN heterostructures Phys. Rev. B, 72, 4, 045316.
- [25] Z.W. Zhou, J.-Xun Sun, M. A. Khan, (2015). Shifted Fang–Howard wavefunction for the two-dimensional electron gas and application to MOSFETs, Int. J. Mod. Phys B.vol 29, 1450250.
- [26] M. Yang et al, (2016). Effect of polarization Coulomb field scattering on parasitic source access resistance and extrinsic transconductance in AlGaIn/GaN heterostructure FETs, IEEE Trans. Electron Devices, 63, 4, 1471–1477.
- [27] L. Hsu and W. Walukiewicz, (2001). Effect of polarization fields on transport properties in AlGaIn/GaN heterostructures, J. Appl. Phys, 89, 1783.
- [28] T. H Yu, K F. Brennan, (2001).Theoretical study of the two-dimensional electron mobility in strained III-nitride heterostructures, J. Appl. Phys, 89, 3827.
- [29] R.yahyazadeh, (2014). Effect of Temperature on the Total Mobility of AlGaIn/GaN High Electron Mobility Transistors ECS Trans, 60, 1,1051-1055.
- [30] J. C. Freeman, (2004). channel temperature model for microwave AlGaIn/GaN power HEMTs on SiC and sapphire, IEEE MTT-S Int. Microwave Symp. Dig. 3, 2031.
- [31] P. Cui, et al, (2018). Effect of different gate lengths on polarization Coulomb field scattering potential in AlGaIn/GaN heterostructure field-effect transistors, Science Reports, 8, 9036.